ISSN 2663-1563 Vol. 8, Issue 1: 37-47, DOI: 10.25236/AJAGE.2026.080105

Experimental and Numerical Investigation on the Tensile and Compressive Performance of Raw Earth Modified with Hydraulic Lime

Jiahui Qu[1,a], Shaoyi Duan[1], Feng Wu[1,b,*]

[1]*School of Transportation Engineering, Dalian Jiaotong University, Dalian, 116028, China*
[a]*2536014108@qq.com,* [b]*wfdjtu@sina.com*
[*]*Corresponding author*

Abstract: *The widespread application of raw earth construction is often hindered by its poor mechanical properties and durability. While chemical stabilization is a common mitigation strategy, the specific reinforcement mechanisms and numerical modeling of hydraulic lime-modified earthen materials remain underexplored. This study investigates the compressive and splitting tensile performance of raw earth matrices stabilized with varying dosages (5% and 10%) of natural and artificial hydraulic limes (NHL and AHL). Experimental results reveal that both stabilizers significantly enhance the mechanical properties of the earth matrix, with the 10% AHL admixture providing the most substantial improvement. Furthermore, a three-dimensional numerical framework based on the Concrete Damaged Plasticity (CDP) model was developed to simulate the macroscopic mechanical responses. The numerical predictions show excellent agreement with the experimental data, particularly for the 10% stabilization groups, accurately capturing the peak strength, post-peak strain-softening behavior, and complex failure modes. These findings validate the applicability of the CDP model for analyzing the non-linear loading behavior and damage evolution of hydraulic lime-stabilized earth, providing a reliable theoretical basis and numerical tool for future earthen heritage conservation and structural design.*

Keywords: *Raw earth; Hydraulic lime; Numerical investigation; Mechanical properties*

1. Introduction

Raw earth construction, which uses natural soil as its primary material, offers advantages such as low-technical construction methods and environmental sustainability through recyclability. However, its practical application is limited by poor durability and mechanical properties[1-4]. Chemical stabilizers enhance soil structure through hydration reactions and ion exchange, significantly improving strength and ductility[5-6]. For instance, waterborne polyurethane can strengthen particle bonding and mechanical strength; its polymer chains penetrate the pores of raw earth, cementing loose soil particles and filling voids[7]. However, due to the high content of fine particles, earthen structures are prone to cracking from excessive drying shrinkage. Additives like polyvinyl alcohol[8] and silicates[9] can rapidly penetrate and bond soil particles. Nevertheless, differences in compatibility with raw earth can lead to interface deterioration[10] and strength degradation upon long-term exposure[11]. In contrast, lime mortar exhibits unique and superior compatibility for strengthening raw earth. Consequently, lime-based materials with better compatibility have emerged as a new direction for improvement[12].

Hydraulic lime (HL) hardens upon contact with water and subsequently gains strength through carbonation in air, while also being able to set and strengthen underwater. It is considered a preferred green modification option due to its rapid hardening, strong adhesion, and good vapor permeability[13]. Hydraulic lime is categorized into natural hydraulic lime and artificial hydraulic lime.

Natural hydraulic lime is produced by calcining argillaceous limestone at 900–1250°C, exhibiting dual hardening characteristics through the formation of C-S-H and $CaCO_3$ during hydration[14]. Research confirms its suitability for repairing raw earth structures due to excellent permeability and interfacial bond strength[15]. Artificial hydraulic lime is obtained by mixing materials containing calcium silicate, calcium aluminate, and calcium hydroxide[16]. While it undergoes some hardening in aqueous environments, approximately 30% of its strength derives from air-hardening components, necessitating the addition of slaked lime during production[17]. Hydraulic lime has been widely used in European historic building restoration. For instance, Sepulcre-Aguilar[18] found that adding white cement to lime

ISSN 2663-1563 Vol. 8, Issue 1: 37-47, DOI: 10.25236/AJAGE.2026.080105

mortars produced hydration products comparable to natural hydraulic lime, making it appropriate for restoration applications.

However, research on hydraulic lime has primarily focused on masonry relic restoration, with many studies still employing air-hardening lime, leading to an incomplete understanding of hydraulic lime. Finite element analysis (FEA)[19-20], a common numerical simulation tool in construction materials research, can replicate stress distribution, deformation evolution, and failure modes through mechanical models. This approach reduces experimental workload and costs while providing robust validation for experimental results and mechanical analysis. In the specific field of hydraulic lime-modified raw earth, current research remains largely confined to physical and mechanical experiments. No studies have yet systematically integrated FEA with physical testing, limiting the understanding of mechanical behavior mechanisms through numerical methods and constraining effective experimental validation.

Therefore, to promote hydraulic lime application in raw earth construction, this study prepared two hydraulic lime types and tested raw earth specimens with varying dosages under compression and splitting tension. Using the Concrete Damage Plasticity (CDP) model in Abaqus, full-process simulations were conducted. Comparing simulated and experimental stress-strain curves and failure modes validated the CDP model's applicability, providing reliable support for engineering design and numerical analysis of modified raw earth materials.

2. Materials and Methods

2.1 Experimental Materials

The following materials were used in this study: (1) Raw earth material: local clay from Dalian, with a natural moisture content of 9%, plastic limit of 15.78%, liquid limit of 42.77%, plasticity index of 26.99, maximum dry density of 1.85 g/cm³, and optimal moisture content of 15%. (2) Natural hydraulic lime: prepared solely from natural Liaojiang stone (calcareous nodule) sourced from Lingshou County, Hebei Province. It was produced by high-temperature calcination in a muffle furnace followed by natural cooling to room temperature. The chemical composition of the calcined powder was determined using X-ray fluorescence spectrometry (XRF)[21], with the main constituents listed in Table 1. (3) Artificial hydraulic lime: formulated by mixing raw materials with a certain degree of whiteness, including air-hardening lime (slaked lime), white cement, ground calcium carbonate powder, and active micro-powder[16]. The air-hardening lime was a commercially available product, appearing as a white crystalline powder with an effective $Ca(OH)_2$ content of 93.5%, a bulk density of 0.9 g/cm³, and a fineness of 200 mesh.

Table 1 Chemical Composition of Natural Hydraulic Lime (wt%).

CFA	C2S	SiO_2	Gln	$CaSiO_3$	Kfs	Ab	Dol	C_3A	CaO
1.8	42.9	23.7	6.4	2.2	5.2	4.7	/	1.2	12.0

2.2 Experimental Methods

The preparation methods for the artificial hydraulic lime (AHLS) and natural hydraulic lime (NHLS) were as follows: AHLS was produced by weighing and mixing slaked lime, white cement, ground calcium carbonate powder, and active micro-powder according to their respective proportions. NHLS was prepared by first cleaning the required Liaojiang stones. After cleaning, the stones were placed into a PE 200*350 small laboratory jaw crusher for size reduction. The crushed material was then passed through an SZS-type three-dimensional vibrating sieve machine; following sieving, a powder with a fineness of 180 mesh was obtained. This powder was subsequently placed into an S11-18-18 box-type sintering resistance furnace, calcined for 3 hours[22], and then allowed to cool naturally to room temperature.

ISSN 2663-1563 Vol. 8, Issue 1: 37-47, DOI: 10.25236/AJAGE.2026.080105

(a) Mixing of materials (b) Curing specimens (c) Molding of test specimens

Figure 1: Specimen Preparation Process.

Mechanical property tests (compressive and splitting tensile) were conducted on small-scale specimens. Compressive tests were performed using a SUNS micro-controlled electro-hydraulic servo universal testing machine (WAW-300) on 70 mm cube specimens. These comprised untreated soil (S0) and chemically stabilized specimens, including artificial hydraulic lime-stabilized soil at 5% and 10% dosages (R1-R2) and natural hydraulic lime-stabilized soil at corresponding dosages (T1-T2). Three specimens per dosage yielded 15 total specimens. Testing and strength determination followed methods proposed by Zhang Kun et al[23] for raw earth materials. The specimen preparation process is shown in Figure 1.

The splitting tensile tests were conducted by placing a steel plate on the base of the testing platform. Ametal bar measuring 5mm×5mm×20 mm was positioned at the center of the steel plate, and the testspecimen was then placed centrally on top of this metal bar. A universal testing machine was used toapply load at a constant rate of 1.0 mm/min, and the ultimate load during the loading process wasrecorded. Following the recording of the load, data processing was performed to calculate the splittingtensile strength of the stabilized specimens. Common testing methods for this purpose include theBrazilian test and the three-point bending test, among others[24].

3. Results Analysis

3.1 Uniaxial Compressive Strength Test Results

Reinforced soil specimens must be cured naturally for 7 days before undergoing compressive testing. The test was conducted using three 70-mm cubic specimens to evaluate the mechanical properties of soil bricks, mud mortar, and consolidated soil matrices[25] .

(a) Crack initiation (b) Crack propagation (c) Surface spalling (d) Specimen collapse

Figure 2: Phenomenon of compressive test.

As shown in the Figure 2, no obvious cracks were observed in the specimens during the initial loading stage. As the load increased, cracks gradually initiated along the stress direction, continuously propagating and coalescing. Concurrently, spalling occurred at the corners, the surface began to bulge, and the outer layer shed. Ultimately, this led to large fragments detaching and overall collapse of the specimen. Following failure, the load did not drop abruptly but decreased relatively rapidly to 80% of the peak load, at which point the test was terminated.

The 7-day compressive strength of the untreated soil was 0.21 MPa, while the maximum value for stabilized specimens reached 0.57 MPa-an increase of up to 239%. The highest overall strength was observed in specimen R10-KY at 28 days, attaining 2.68 MPa. Strength development in natural hydraulic lime-stabilized soil accelerated after 28 days, whereas artificial hydraulic lime-stabilized soil exhibited rapid early strength gain (7-28 days) followed by slower later growth. This indicates that artificial lime

ISSN 2663-1563 Vol. 8, Issue 1: 37-47, DOI: 10.25236/AJAGE.2026.080105

contributes predominantly to early-stage strength formation, while natural lime plays a more significant role in later stages. Moreover, artificial hydraulic lime R10-KY (e.g., Figure 3) demonstrated superior stabilization performance compared to its natural counterpart. Specimens stabilized with 5% hydraulic lime showed a 13%-30% reduction in strength relative to untreated soil. This decline is attributed to insufficient hydraulic dosage, which fails to generate enough cementitious products to form a continuous binding network. Incomplete hydration, weak particle bonding, increased porosity, and early-age shrinkage further disrupted the original dense structure of the soil matrix. In contrast, specimens stabilized with 10% hydraulic lime exhibited clear and substantial strength improvement.

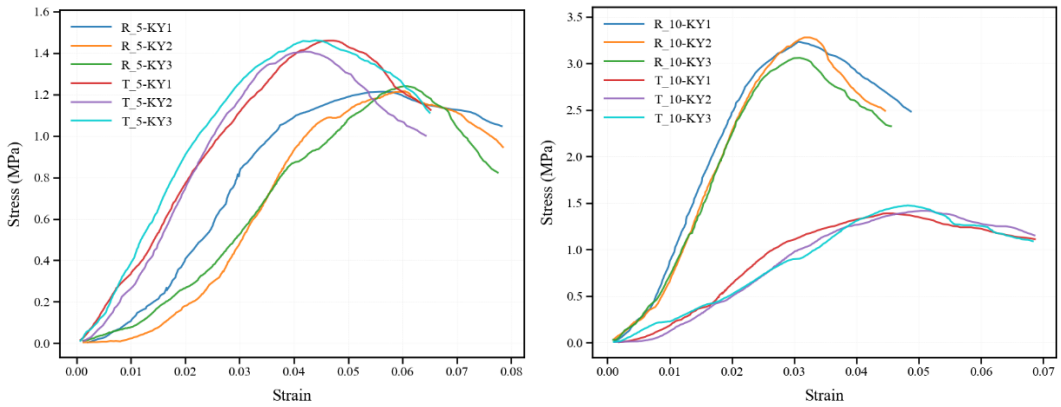

(a) Reinforcement agent content 5% *(b) Reinforcement agent content 10%*

Figure 3: Compression Test Stress-Strain Curve.

Hydraulic lime was found to enhance the compressive strength of raw earth to varying degrees. The compressive strength of the untreated soil was 1.2 MPa, while the minimum increase observed among the stabilized specimens was 2% (reaching 1.23 MPa). Artificial hydraulic lime significantly outperformed natural hydraulic lime in terms of strengthening effectiveness, with the R10-KY formulation demonstrating superior performance.

3.2 Splitting Tensile Test Results

All specimens were cast using the two-end clamps of the testing machine. It is important to note that the specimens were placed vertically to avoid any damage caused by bending. Finally, the pull-out tests were conducted using an electronic universal testing machine at a constant displacement rate of 1.0 mm/min[26]. The calculation formula for splitting tensile strength was originally intended for 150 mm cube specimens. Since this experiment used 70 mm cube specimens, the final calculated results were multiplied by a size conversion factor of 0.85 to correct for the dimensional difference[27].

(a) Specimen placement (b) Crack formation (c) Through crack (d) Specimen failure

Figure 4: Splitting Test Phenomena.

As shown in Figure 4., after preloading, the specimen was loaded until failure. Initial non-penetrating cracks appeared along the vertical plane of the metal bar, eventually forming a penetrating main crack with secondary fissures, followed by a sharp load drop at complete fracture.

The 7-day splitting tensile strength of untreated soil was 0.009 MPa. All stabilized groups showed improvement, with T5-PL increasing least and R10-KY most significantly. At 28 days, untreated strength reached 0.038 MPa, with T5-PL again showing minimal gain—even exhibiting negative growth due to slow stabilizer reaction—while R10-KY achieved six times the untreated strength, attributed to cement content in its stabilizer enabling rapid early development. After 60 days, R10-KY maintained the highest

ISSN 2663-1563 Vol. 8, Issue 1: 37-47, DOI: 10.25236/AJAGE.2026.080105

increase at approximately four times untreated strength.These results align with mechanical evolution trends, confirming that artificial hydraulic lime relies primarily on later-stage curing for strength formation—distinct from cement-based materials' early strength development pattern.

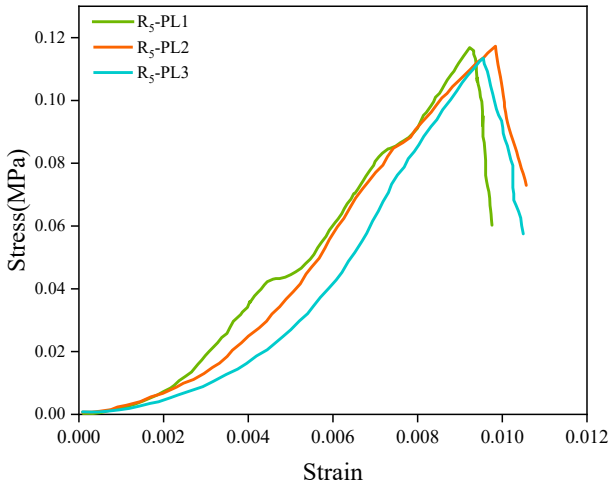

Figure 5: Splitting tensile strength of partial reinforcement.

From the load-displacement curve of the splitting test shown in Figure 5, it can be seen that the slope exhibited an initially small slope that gradually increased. Upon reaching peak load, a sudden drop occurred indicating failure. Following failure, the specimens retained some residual load-bearing capacity with a rapid load decline, attributed to incomplete cracking and ongoing interfacial friction. The first peak load was adopted as the basis for calculating splitting tensile strength.

4. Analysis of the Constitutive Model for the Natural Soil Matrix

4.1 Model Development

In the finite element analysis conducted with ABAQUS, the constitutive models commonly used for concrete materials fall into three main categories: the smeared crack model, the brittle crack model, and the concrete damaged plasticity (CDP) model. Among these, the CDP model, which couples plastic deformation with damage evolution, effectively captures the strength degradation, damage accumulation, and inelastic behavior of concrete under complex loading conditions[28]. In this study, a three-dimensional solid geometric model was established in Abaqus/CAE based on the experimental specimen dimensions (70 mm×70 mm×70 mm). An eight-node linear reduced-integration solid element (C3D8R) was selected for mesh generation. A structured meshing technique was applied to the entire specimen with a global mesh size of 4 mm, ensuring that all element aspect ratios remained below 0.8, as shown in Figure 6.

For the splitting tensile test simulations, the contact interaction between the metal loading strips and the specimen was modeled. Following the experimental setup, rigid loading strips measuring 5 mm×5 mm×70 mm were positioned on the top and bottom surfaces of the model and meshed using discrete rigid elements (R3D4). Each loading strip was centered on the specimen surface to ensure accurate load transfer along the splitting plane. The interface between the strips and the specimen was defined as "surface-to-surface contact." Tangential behavior was set to "rough" to prevent relative slip, while normal behavior was defined as "hard contact," allowing separation after contact to simulate specimen splitting. For both compressive and splitting tensile simulations, the "Static, General" procedure type was employed, as it is suitable for capturing the large deformations and contact separation behavior expected in the specimens.

ISSN 2663-1563 Vol. 8, Issue 1: 37-47, DOI: 10.25236/AJAGE.2026.080105

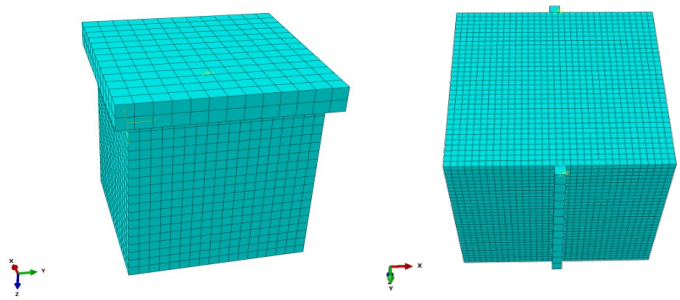

(a) Compressive Specimen Model *(b) Splitting Test Specimen Model*

Figure 6: Grid division.

4.2 Parameter Settings

During the elastic loading stage of concrete, the CDP model directly describes the material's mechanical properties using the initial elastic modulusE_0 . When concrete enters the damage stage, the elastic modulus expression becomes:

$$E = (1 - d_c)E_0 \tag{1}$$

$$E = (1 - d_t)E_0 \tag{2}$$

In the formula, dc and dt represent the compressive and tensile plastic damage factors, respectively, with a value range of [0,1]. A value of 1 indicates that the concrete is completely damaged and has entirely lost its strength, while 0 indicates that no damage has occurred in the concrete. E0 is the initial elastic modulus of the concrete. Given that raw earth exhibits an initial pore compaction stage, the linear ascending segment of the stress-strain curve was selected for determining E0. For instance, in the compressive curve of the R10 specimen, the secant modulus corresponding to the stress range of 0.5-3.0 MPa was obtained through linear fitting, yielding E0=100 MPa. For the splitting tensile simulation, based on the stress range of 0.1-0.5 MPa for the R5 specimen from the compressive tests, fitting resulted in E0=80 MPa. According to the influence of CDP model parameters in uniaxial tension-compression simulations by Shi Xinyu et al[29], and in conjunction with the experimental data from this study, Poisson's ratio υ was selected as 0.2. After multiple tests, the other model parameters are determined as shown in Table 2.

Table 2 Model Parameters.

Parameter	*Expansion angle*	*Eccentricity*	*Biaxial Compression vs. Uniaxial Compression Ratio of ultimate compressive strengths*	*Constant stress ratio*	*Viscosity coefficient*
Value	*30*	*0.1*	*1.16*	*0.66667*	*1E-05*

The dilation angle and eccentricity are parameters associated with the flow rule governing the yield surface. The parameter K influences the shape of the concrete yield surface. The term fb0 represents the concrete's biaxial compressive strength, while fc0 denotes its uniaxial compressive strength; the ratio of these two values is adopted according to the recommended values from relevant standards. The viscosity parameter μ, defined within the CDP model, affects the convergence behavior of the analysis: larger values of μ facilitate easier convergence, whereas smaller values enhance computational accuracy. A value of μ=0.00001 was selected in this study to simultaneously satisfy both accuracy and convergence requirements.

Regarding the calculation of damage factors, directly incorporating the damage evolution parameters provided by design codes into the CDP model often leads to difficulties in achieving computational convergence. Consequently, the method for calculating damage factors proposed by Sidoroff, based on specific underlying assumptions, was generally adopted[30-31]:

$$d_c = 1 - \sqrt{\frac{\sigma_c}{E_0 \varepsilon_c}} \tag{3}$$

ISSN 2663-1563 Vol. 8, Issue 1: 37-47, DOI: 10.25236/AJAGE.2026.080105

$$d_t = 1 - \sqrt{\frac{\sigma_t}{E_0 \varepsilon_t}} \tag{4}$$

Using this method, the numerical simulation results yield a smooth curve and converge easily. Here, σ and ε are obtained from experiments;E_0 is the initial elastic modulus of concrete.

4.3 Comparison and Analysis of Simulation Results with Experimental Data

The analysis of the stress field distribution indicates that the splitting failure of the modified raw earth specimens is dominated by tensile stress along the central vertical section. The stress transfer patterns and stress concentration regions obtained from the numerical simulation are in good agreement with both the theoretical solution of the Brazilian splitting test and the failure morphologies observed in the experiments. As shown in Figure 7(b) that high compressive stress zones are concentrated at the contact areas between the upper/lower loading steel strips and the specimen surface, which conforms to the contact stress distribution law of an elastic body under line loading. As the stress extends inward along the specimen's axial direction, the compressive stress level rapidly attenuates.

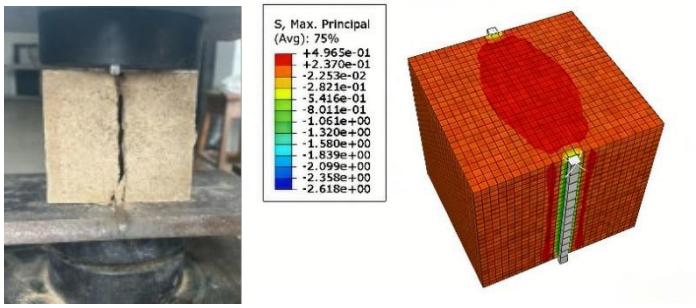

(a) Comparison of Splitting Failure Modes

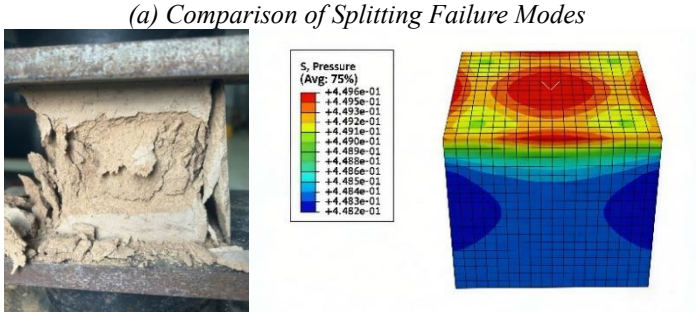

(b) Comparison of Compressive Failure Modes

Figure 7: Comparison of Failure Modes.

As shown in Figure 7(a), in the uniaxial compression tests, the specimens ultimately developed a single diagonally penetrating main crack. The numerical simulation results demonstrate that specimen failure is concentrated within a single diagonal banded zone, showing a high degree of consistency with the main crack observed experimentally. This indicates that under uniaxial compression, the specimen does not undergo uniform axial compressive failure; rather, under the action of axial compressive stress, once the shear stress on the oblique section reaches the shear strength of the soil matrix, shear slip failure occurs along that inclined plane. In summary, under both splitting tensile and uniaxial compressive loading conditions, the failure modes obtained from numerical simulations exhibit good consistency with those observed in the experiments.

4.4 Verification of Numerical Simulation

Concrete exhibits complex nonlinear behavior under compression, which is captured by constitutive models based on damage mechanics, plasticity theory, or a combined damage-plasticity framework[32]. For instance, the elastoplastic constitutive model incorporating damage effects developed by Ma Xueyi et al. accurately reproduces the nonlinear mechanical characteristics and damage evolution of concrete throughout the entire compressive process[33]. In this study, using measured basic mechanical parameters of raw earth as model inputs, a refined numerical simulation of the complete uniaxial compressive process was conducted to systematically analyze its damage evolution laws and characteristics under loading.

ISSN 2663-1563 Vol. 8, Issue 1: 37-47, DOI: 10.25236/AJAGE.2026.080105

As shown in the Figure 8, comparison between the experimental and simulated stress-strain curves for the untreated soil specimen demonstrates high consistency. In the linear elastic stage: soil, as a typical compacted porous medium, exhibits a distinct initial compaction segment at the beginning of loading, manifested macroscopically as a concave-upward nonlinear curve. Since the numerical simulation cannot effectively replicate this compaction process, the simulated curve was directly compared with the linear ascending phase of the experimental curve. Regarding the plastic yielding and peak strength stage: following the elastic stage, the experimental curve enters a plastic yielding hardening phase until reaching peak strength. The numerical simulation accurately reproduces the mechanical response of this stage, with highly consistent peak strength and peak strain values.In the post-peak softening stage: both curves exhibit strain-softening characteristics, with stress decreasing rapidly as strain increases after the peak, showing a highly consistent downward trend.

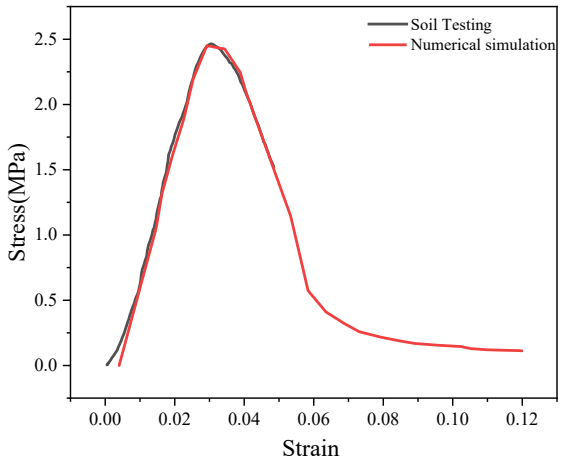

Figure 8: Comparison of Stress-Strain Curves.

Comparative analysis of experimental and numerical stress-strain curves for hydraulic lime-stabilized specimens reveals dosage-dependent simulation accuracy. For the 10% natural hydraulic lime specimen (T10, Figure 9), the simulated curve closely matches the experimental curve during elastic ascent, with consistent linear trends and strong agreement in peak stress and strain, accurately capturing ultimate load capacity. In the post-peak stage, the softening and descent rate align well with experimental observations without significant deviation.For the 10% artificial hydraulic lime specimen (R10, Figure 9), even better agreement is observed. The linear elastic slopes are nearly identical, peak point coincidence is higher, and verification of ultimate compressive strength is more accurate than for T10. Additionally, the simulated curve fully captures the gentle post-peak descending trend, closely matching the material's actual plastic damage development.

In contrast, specimens stabilized with 5% hydraulic lime (R5 Figure 9, T5 Figure 9) show notably weaker fitting between simulated and experimental curves. This is attributable to insufficient hydration at low dosages: inadequate generation of hydration products fails to fill internal pores and achieve stable interparticle cementation, resulting in poor uniformity of pore structure and particle bonding. This induces localized heterogeneity in stress transfer and damage development during loading, causing local fluctuations in experimental stress-strain curves and deviations from continuum-based simulation results.

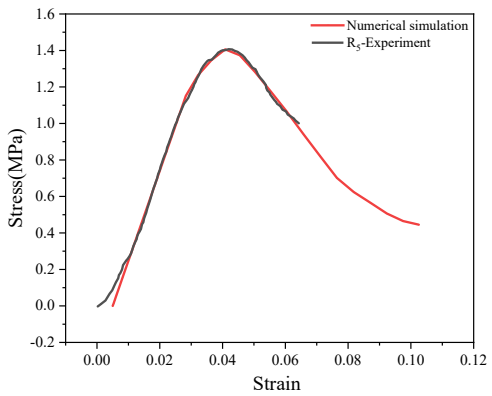

(a) R5 comparison diagram

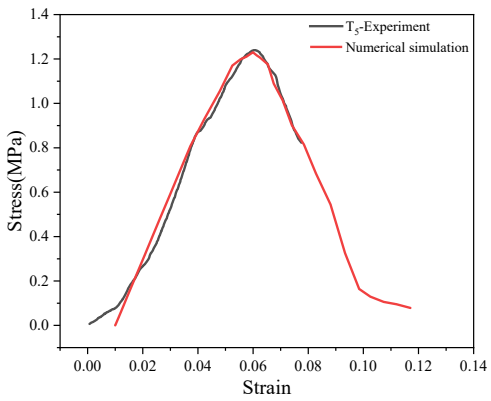

(b) T5 comparison diagram

ISSN 2663-1563 Vol. 8, Issue 1: 37-47, DOI: 10.25236/AJAGE.2026.080105

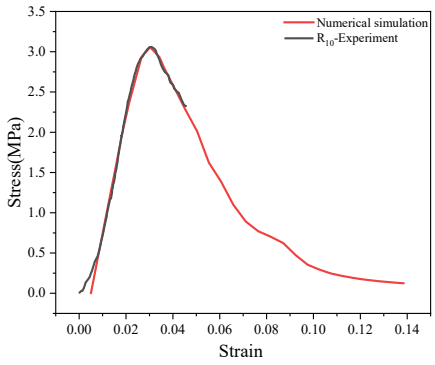

(c) R10 comparison diagram

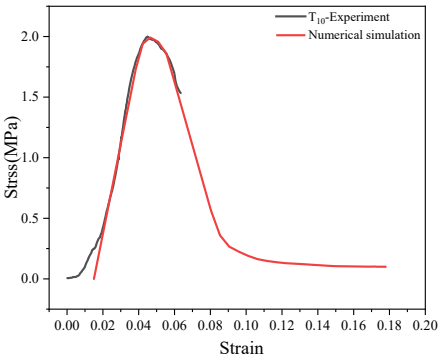

(d) T10 comparison diagram

Figure 9: Comparison of Simulation and Experimental Results.

Overall, the established numerical model effectively validates the mechanical behavior of hydraulic lime-modified raw earth throughout the uniaxial compression process, demonstrating high simulation accuracy for 10% lime content specimens—which exhibit superior modification effects—and providing reliable support for subsequent numerical analyses.

For splitting tensile tests, the fracture failure of quasi-brittle materials like raw earth, where tensile strength is far lower than compressive strength, is governed by maximum tensile stress: cracking occurs once this stress reaches the material's tensile strength. Taking the 5% hydraulic lime-modified specimen as an example, the Figure 10 compares the experimental stress-strain curves (three parallel specimens) with ABAQUS simulation results. Based on the continuous, homogeneous medium assumption, the model simplifies modified raw earth into an ideal continuum without initial pores or material heterogeneity, assuming a uniformly dense initial state. The constitutive relationship's initial deformation corresponds to linear elastic deformation of the material matrix, failing to account for progressive closure of discrete pores and micro-cracks. Additionally, since the constitutive model employs a constant elastic modulus, it cannot replicate the initial-stage nonlinear behavior where equivalent stiffness increases with strain, resulting in slight but acceptable deviations between simulated and experimental curves.

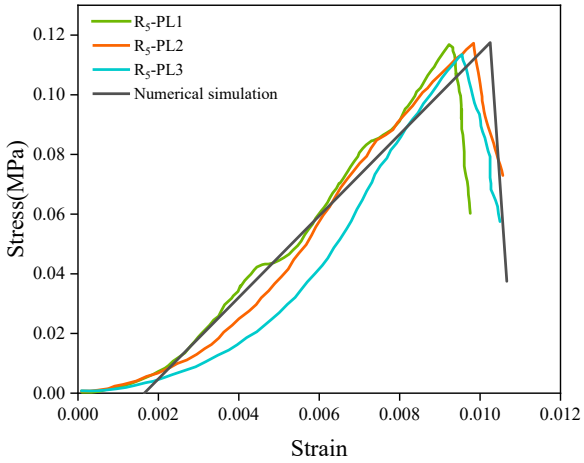

Figure 10: Comparison diagram of splitting tests.

Although the numerical simulation curve is unable to replicate the nonlinear deformation characteristics in the initial loading stage—governed by pore compaction and material heterogeneity—due to the inherent limitations of the continuum homogenization assumption and the constitutive model, the simulation results exhibit strong agreement with the experimental measurements in terms of three key mechanical indicators: peak strength, peak strain, and post-peak brittle drop. The simulation accurately captures the ultimate tensile capacity, critical failure deformation threshold, and post-peak damage degradation behavior of the 5% hydraulic lime-modified raw earth specimens. This demonstrates that the reasonable simplification of initial non-structural deformation does not compromise the model's reliable characterization of the core tensile mechanical behavior of the modified raw earth.

ISSN 2663-1563 Vol. 8, Issue 1: 37-47, DOI: 10.25236/AJAGE.2026.080105

5. Conclusions

This study investigated the modification effects of natural and artificial hydraulic lime on Dalian local clay through mechanical tests and CDP-based numerical simulations. Key conclusions are:

(1) A dosage threshold exists for effective modification. At 5% lime content, insufficient hydration products reduced compressive strength by 13%-30% compared to untreated soil. At 10% content, both lime types effectively filled pores and enhanced interparticle bonding, significantly improving mechanical performance.

(2) Artificial and natural hydraulic lime exhibit distinct strength evolution patterns. Artificial lime gains strength rapidly in early curing (7-28d), achieving 2.68 MPa compressive strength at 28d (239% increase) and 6 higher splitting tensile strength than untreated soil. Natural lime develops strength more slowly initially but accelerates during 28-60d, suiting long-term reinforcement applications. The 10% artificial lime formulation showed optimal modification effects.

(3) The CDP-based numerical model accurately simulated 10% lime-modified specimens, with peak strain errors below 3% and consistent post-peak softening trends. While splitting tensile simulations couldn't replicate initial nonlinear deformation, core mechanical indicators (peak strength/strain, post-peak behavior) matched experimental results well.

(4) Simulations successfully reproduced failure mechanisms: tension-dominated mid-section failure in splitting tests aligned with damage zones, while diagonal shear slip failure in compression matched plastic strain concentrations. These consistencies validate the model parameter selection.

Future work should refine dosage gradients for optimal modification intervals and investigate long-term performance under complex environments to support engineering applications.

References

[1] Jing Qimin. Earthen Architecture [J]. Architectural Journal, 1994(5): 43-47.
[2] Wang Fengrui, Wang Xudong, Wang Jie, et al. Study on the Structure and Properties of Earthen Materials Modified with Kaolin-Based Composite Reinforcing Agents [J].Journal of Lanzhou University (Natural Science Edition), 2020, 56(03): 341-348. DOI: 10.13885/j.issn.0455-2059.2020.03.008.
[3] Wang Yihong, Liang Jian, Zhang Xiangying, et al. A Review of Research on Earthen Structures in China [J]. Journal of Civil Engineering, 2015, 48(05): 98-107. DOI:10.15951/j.tmgcxb.2015.05.012.
[4] Tang Weidong, Zhao Zhuo, Chen Zihao, et al. Experimental Study on Early-Age Crack Resistance and Mechanical Properties of Fiber-Reinforced Concrete [J]. Henan Science, 2017, 35(04): 606-610.
[5] Imanzadeh S, Jarno A, Hibouche A, et al. Ductility analysis of vegetal-fiber reinforced raw earth concrete by mixture design [J]. Construction and Building Materials, 2020, 239: 117829.
[6] Guo Xingchen. Experimental Study on the Shear Mechanical Properties of Plant Fiber-Modified Raw Earth Masonry [D]. Xinjiang University, 2021. DOI:10.27429/d.cnki.gxjdu.2021.000350.
[7] Zhao W, Wang Y, Tian Q, et al. Unconfined mechanical properties and micromechanism of short-age recycled aggregate from road solid waste modified by waterborne polyurethane[J]. Materials Research Express, 2024, 11(1): 015503.
[8] Zhang Q, Chen W, Fan W. Protection of earthen sites through soil hydrophobicity under freeze–thaw and dry–wet cycles[J]. Construction and Building Materials, 2020, 262: 120089.
[9] Chen W, Zhang Y, Zhang J, et al. Consolidation effect of composite materials on earthen sites[J]. Construction and Building Materials, 2018, 187: 730-737.
[10] Pan C, Chen K, Chen D, et al. Research progress on the in-situ protection status and technology of earthen sites in humid environments[J]. Construction and Building Materials, 2020, 253: 119219.
[11] Shao M, Li L, Chen W, et al. Investigation and modification of two types of traditional Chinese lime in cultural heritage sites[J]. Journal of Cultural Heritage, 2019, 36: 118-127.
[12] Zhu H, Wu X, Chen J, et al. Effectiveness and compatibility of fabricated hydraulic lime prepared with ultrafine pozzolanic materials in consolidating soil-matrix[J]. Construction and Building Materials, 2023, 378: 131105.
[13] Gu L, Shang H, Wu Y, et al. Research on the Application of Metakaolin in Artificial Hydraulic Lime Restoration Mortar [J].Silicate Bulletin, 2023, 42(12): 4351–4359+4367. DOI: 10.16552/j.cnki.issn1001-1625.2023.12.008.
[14] Apostolopoulou M, Bakolas A, Kotsainas M. Mechanical and physical performance of natural hydraulic lime mortars [J]. Construction and Building Materials, 2021, 290: 123272.
[15] Bras A, Henriques F M A. Natural hydraulic lime-based grouts—The selection of grout injection

ISSN 2663-1563 Vol. 8, Issue 1: 37-47, DOI: 10.25236/AJAGE.2026.080105

parameters for masonry consolidation[J]. Construction and Building Materials, 2012, 26(1): 135-144.
[16] Duan Shao-yi. Study on the Mechanical Properties of Hydraulic Lime Reinforced Earthen Materials [D]. Dalian Jiaotong University, 2023. DOI:10.26990/d.cnki.gsltc.2023.000792.
[17] German Institute for Stone Conservation Research Report No. 1 / IFS-Bericht Nr. 1: Hydraulic Limes for Monument Conservation (Research on Hydraulic Limes in Monument Conservation), 1998.
[18] Sepulcre-Aguilar A, Hermandez-Olivares F. Assessment of Phase Formation in Lime-Based Mortars with Added Metakaolin, Portland Cement, and Sepiolite for Grouting of Historic Masonry [J]. Cement and Concrete Research, 2010, 40(1): 66-76.
[19] Li Zhengjian. Numerical Simulation Study on the Mechanical Properties of Fiber-Reinforced High-Performance Concrete [J]. Concrete, 2023, (06): 109-114.
[20] Zeng Y, Guo H, Lei J, et al. Study on the mechanical properties of recycled brick coarse aggregate concrete based on finite element modeling [J]. Journal of Building Engineering, 2024, 95: 110110.
[21] Luo Kai. Design, Preparation, and Performance Study of Natural Hydraulic Lime [D]. Southwest University of Science and Technology, 2020. DOI: 10.27415/d.cnki.gxngc.2020.000982.
[22] Yang Jianlin, Song Wenwei, Wang Laigui, et al. Study on the Synthesis and Physical and Mechanical Properties of Jiangshi Hydraulic Lime [J]. Journal of Rock Mechanics and Engineering, 2018, 37(07): 1766-1775. DOI: 10.13722/j.cnki.jrme.2017.1526.
[23] Zhang Kun. A Study on Standard Test Methods for the Strength of Earth-Based Materials [D]. Chang'an University, 2017.
[24] Liao Z Y, Zhu J B, Tang C A. Numerical investigation of rock tensile strength determined by direct tension, Brazilian, and three-point bending tests [J]. International Journal of Rock Mechanics and Mining Sciences, 2019, 115: 21-32.
[25] Han W, Wu F, Cheng Y, et al. Compressive Performance of Adobe Masonry Strengthened with Glass-Fiber-Reinforced Matrix Composites [J]. Materials and Structures, 2023, 56(3): 53.
[26] Han W, Wu F, Zhao Y, et al. Experimental Study on Bond Behavior of Glass Textile Mesh in Earth-Based Matrix[J]. Materials, 2023, 16(3): 1161.
[27] "Standard Test Methods for Mechanical Properties of Ordinary Concrete" GB/T50081-2002. Beijing, China Academy of Building Research, 2007-01-01.
[28] Zhang Tian, Hou Zhengmeng, Li Xiaoqin, et al. Research on the Calculation Method of Parameters for Concrete Plastic Damage Models [J]. Journal of Computational Mechanics, 2024, 41(06): 1130-1137.
[29] Shi Xinyu, Yao Yan, Wang Ling, et al. Influence of CDP Model Parameters Based on Uniaxial Tensile-Compressive Simulation [J]. Building Structures, 2021, 51(S2): 999-1007.
[30] Christoforo A L, Arroyo F N, De Sousa A M D, et al. Concrete Damaged Plasticity (CDP) adjustment parameters for the application in simulations of timber or wood composite structures [C]//Structures. Elsevier, 2025, 73: 108334.
[31] Ağcakoca E, Jueyendah S, Yaman Z, et al. Advanced Hybrid Modeling of Cementitious Composites Using Machine Learning and Finite Element Analysis Based on the CDP Model [J]. Buildings, 2025, 15(17): 3026.
[32] Raza A, Khan Q U Z, Ahmad A. Numerical investigation of load-carrying capacity of GFRP-reinforced rectangular concrete members using the CDP model in ABAQUS[J]. Advances in Civil Engineering, 2019, 2019(1): 1745341.
[33] Saidongla Ma Xueyi, Cui Wei, Jiang Zhi'an, et al. Development and Numerical Implementation of a Plastic Concrete Constitutive Model Considering Damage Effects [J]. Journal of Hydraulic Engineering, 2025, 56(07): 920–932. DOI:10.13243/j.cnki.slxb.20240585.